Composites: Part A 171 (2023) 107559

Contents lists available at ScienceDirect

Composites Part A

journal homepage: www.elsevier.com/locate/compositesa

Shape memory polymer composite circular and square hollow members for deployable structures

K.D.C. Emmanuel [a,b], L.H.J. Jeewantha [a,b], H.M.C.M. Herath [c], J.A. Epaarachchi [a,b,*], T. Aravinthan [a,b]

[a] School of Mechanical and Electrical Engineering, Faculty of Health Engineering and Sciences, University of Southern Queensland, Toowoomba, Australia
[b] Centre for Future Materials, University of Southern Queensland, Toowoomba, Australia
[c] Department of Engineering Technology, Faculty of Technological Studies, Uva Wellassa University, Badulla, Sri Lanka

ARTICLE INFO

Keywords:
Fatigue behavior
Shape memory polymer composites
Deformable structural components
Smart constructions
Deployable structures

ABSTRACT

The exciting shape memorizing ability of shape memory polymer composites (SMPCs) has attracted the interest of researchers catering to the needs of modern constructions. As well as outer space related applications, SMPCs can be used effectively in civil construction techniques. SMPC integrated structures have the capability to deform into a compact shape for easy transportation to site where they can be recovered to their original shape. This paper details the application of the shape memory effect (SME) in glass SMPC circular and square hollow (CHS and SHS) structural members and SMPC incorporated deployable structures. The SME of SMPC members were analysed numerically via ABAQUS software and validated with experimental results. It was revealed that SMPC SHS and CHS integrated large scale structures can be temporarily deformed to achieve a volume saving of 52 % and 70 %, respectively, for easy handling and transportation. Furthermore, the tension–tension fatigue properties of glass and basalt SMPCs were characterized, and the fatigue study provides significant knowledge to an untouched branch of SMPC performance. We believe that these findings will transform current construction strategies into a new approach, making modern day constructions smarter, quicker and cheaper.

1. Introduction

With advancements in construction technology, engineers look for opportunities to develop new construction methods and adopt novel building materials. Such improvements can enhance construction speed, minimize labour requirements, produce less carbon dioxide (CO_2) emissions, and allow people to live in safe and affordable homes. So far, cement, steel, and wood have been used extensively as building materials [1,2]. In addition, traditional construction methods offer very slow construction speeds and are labour intensive. Consequently, the need for new building materials and efficient technologies are increasing day by day. Interestingly, polymer composites have become a successful substitute construction material and are used in a wide variety of structural applications [3]. Importantly, compared to other materials, smart materials such as shape memory polymer composites (SMPCs), have also shown an impressive and unique performance in engineering applications [4,5].

Shape memory polymers (SMP) is a smart branch of polymers, comprising a unique shape memorizing ability [6]. Unlike traditional polymer materials, SMPs can undergo substantial deformation and retain their temporary compact shape when exposed to an external stimulus [7,8]. SMPs have the ability to recover their initial shape when triggered with the same external stimulus. Researchers have developed different types of shape memory materials that are responsive to external stimuli such as heat, electricity, a magnetic field, microwaves, moisture and light. Heat activation is the most typical stimulus of SMPs and has been extensively studied [9]. To mitigate the poor mechanical properties of SMPs, fibre reinforcements have been incorporated to improve their structural performance [9–13]. Hence, SMPCs with both good structural and shape memory properties can be used effectively in a wide variety of strength demanding applications.

To date, fibre reinforced SMPCs have mainly been developed for outer space exploration applications. The major challenges of conventional structures made of common materials, such as heaviness, high cost and high volume consumed, can be prevented by using lightweight smart SMPC components [14]. SMPCs have also been proposed for use in

* Corresponding author at: School of Mechanical and Electrical Engineering, Faculty of Health Engineering and Sciences, University of Southern Queensland, West Street, Toowoomba, QLD 4350, Australia.
E-mail address: Jayantha.Epaarachchi@usq.edu.au (J.A. Epaarachchi).

https://doi.org/10.1016/j.compositesa.2023.107559
Received 21 January 2023; Received in revised form 23 March 2023; Accepted 6 April 2023
Available online 8 April 2023

deployable lunar habitats to revolutionize rapidly developing space exploration technologies [15]. Moreover, the same concept of incorporating SMPCs can be used in challenging civil applications to enhance construction efficiency. Prefabricated modular construction is a rapidly developing building technology ideal for congested cities where space and time are critical considerations [16]. Despite their remarkable benefits, the handling and transporting of heavy and oversized prefabricated modules have become prominent drawbacks [17]. Also, constructing footbridges in remote areas and challenging terrain requires a lot of labour, time and can become costly. Similarly, the manufacturing and transportation costs of curved and heavy steel beams are very high [18].

However, less attention has been given to integrating SMPCs into structural members such as circular and square hollow (CHS and SHS) sectioned components. Importantly, SMPC CHS and SHS structural components are lightweight, strong and deformable. In addition, to date, most of the research on SMPCs has been limited to low thicknesses (less than 2 mm) and small scaled prototypes. As a result, in our recent work, we studied the adverse effects of increasing the thickness and fibre content of SMPCs on shape programming efficiency. A technique to identify the damage onset stress of SMPCs during programming has also been presented based on finite element analysis (FEA). Interestingly, it was found that programming damage initiates at a compressive stress of 70 MPa and cracks form on the tensioned side beyond 100 MPa [19]. Moreover, research on the durability of SMPCs under fatigue conditions is lacking, as SMPCs have not been proposed for civil constructions.

This article presents the next phase of our recent studies on the development of shape deformable and recoverable SMPC structural members. The structures made from SMPCs are lightweight and can be deformed into a temporary compact shape, allowing easy transportation and handling. Then, the SMPC components can be recovered on the construction site and can be used easily in constructions. They can also be used in the construction of outer space habitats. Consequently, real scale SMPC CHS and SHS components were fabricated, deformed and tested as a proof of concept. The characterization of SMPC fatigue properties which is vital for a construction material is also presented. Importantly, the proposed experimental and FEA framework address some of the exciting and modern SMPC related research aspects which have not been studied adequately. Further, the validated FEA modelling introduces a combination of the material's strength and viscoelastic properties which enables the study of developing stress during programming. The outcomes of this research provide firsthand knowledge of SMPC application in structural components that can be used to remedy current construction challenges. Further, the proposed concepts can be developed to transform traditional, time consuming and costly building procedures into fast paced smart constructions.

2. Materials and methods

2.1. Materials

An epoxy based SMP was synthesized by mixing Bisphenol A epoxy resin Araldite GY 191 with the hardeners Triethylenetetramine (TETA) and Jeffamine D230 to a weight ratio of 13.03: 1: 1.63, respectively. The resin and hardeners were purchased from Huntsman and Sigma-Aldrich, respectively. During fabrication, all SMPCs were initially cured for 24 hrs at room temperature and post cured at 100 °C for 1.5 hrs and at 130 °C for 1 hr.

The SMPC material parameters such as the thickness, reinforcement layers and their orientations were based on the Taguchi optimization presented in our previous study to prevent programming damage. The study showed that excessive compression stress (>70 MPa) can cause three types of visible damage during the programming stage of SMPCs. Also, the storage onset programming temperature (T_S) and rubbery onset temperature of the optimized SMPC were 60 °C and 90 °C, respectively [19].

2.2. Fatigue testing

The fatigue behavior of the optimized SMPCs under tension–tension cyclic loading was investigated in MTS 810–100 kN according to ASTM D3479/D3479M-19 [20]. The specimens were cycled between their minimum and maximum tensile load (stress) under a load control mode at 1 Hz frequency (f). A low frequency was selected to avoid a temperature increase in the sample. The fatigue lives of the SMPC samples were studied for a stress ratio (r = ratio of minimum and maximum stress) of 0.1 and for five selected load levels (L) of 40, 50, 60, 70 and 80 % of ultimate tensile stress (S_{UTS}). The SMPC samples were tabbed to avoid premature failure within the grips along with a 10 Hz data acquisition rate. The tabs were manufactured according to the test standard guidelines from a general purpose polymer reinforced with glass fibre. The load mean (L_M) and amplitude (L_A) were used to define the 'Sine' wave form in the test setup, and the respective values for the glass SMPCs are given in Table 1.

2.3. Temperature effect testing

The SMPC is programmed at the storage onset temperature (T_S = 60 °C). For the material setup of the ABAQUS software, the experimentally measured tensile properties were used to define the SMPC's elastic properties at the programming temperature. Hence, the tensile properties of the optimized SMPCs were only evaluated at the programming temperature of 60 °C. Tests were carried out in MTS 100 kN along with its thermal chamber to maintain the required temperature during the test. As the matrix becomes soft when heated, tabs were attached to the SMPC tensile samples to avoid sample slip and undesirable damage within the fixtures. A reinforced polymer composite with a higher glass transition temperature (T_g) was used as the tab material. A laser extensometer with two reflective tapes positioned 25 mm apart (as shown in Fig. 1) were used to measure the axial strains during tensile testing.

2.4. Fabrication of CHS and SHS members

Two specially designed molds (shown in Fig. 2) were used to fabricate the glass fibre reinforced SMPC CHS and SHS structural members of length 250 mm. The mandrels and outer fixtures were precisely machined to maintain a 3 mm constant thickness in all SMPC components. Additionally, 3 mm spacers were used to position the inner mandrel and restrict its movements inside the mold.

To avoid air bubbles becoming trapped in creating dry patches and to monitor the resin level inside the mold, a resin infusion tube connected to the bottom of the mold was used for pouring the polymer. The pressure differential in the resin infusion tube facilitated an effective and trouble free resin flow when casting the SMPC structural components. Once the molds were filled with SMP, the curing cycle mentioned in Section 2.1 was utilized to fully cure the SMPC components. The key components of the developed mold are listed in Table 2. Subsequently, the fabricated CHS and SHS components were demolded and cut into the lengths required for shape memory testing. Fig. 3 presents manufactured the SMPC CHS and SHS specimens along with their cross sectional dimensions.

Table 1
Load values for glass SMPC fatigue test setup.

SMPC	S_{UTS} (MPa)	r	L %	L_M (kN)	L_A (kN)
Glass	231.9	0.1	80	7.7	6.3
			70	6.7	5.5
			60	6.0	4.9
			50	5.0	4.1
			40	4.0	3.3

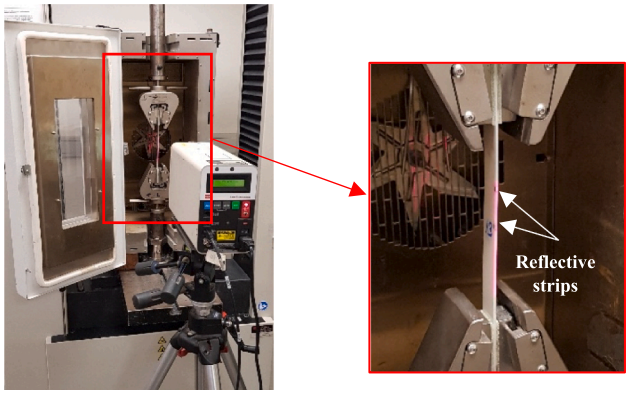

Fig. 1. Elevated temperature tensile experimental setup with laser extensometer and reflective tapes.

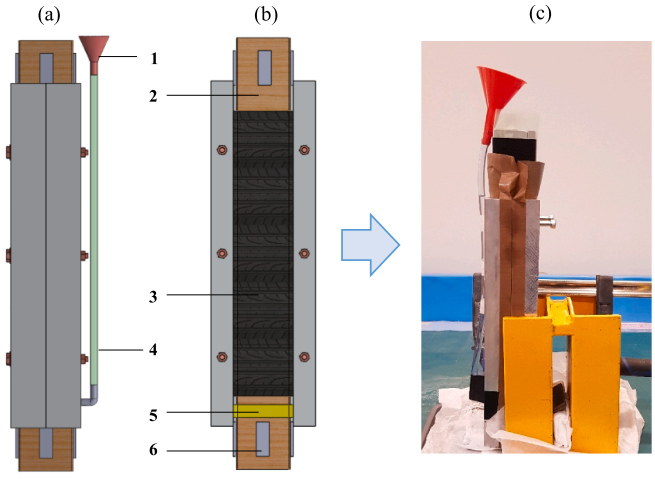

Fig. 2. Solid model and actual manufacturing technique of SHS SMPC members; (a) side view (b) inside view of the mold (c) actual fabrication setup.

Table 2
Components of the customized mold.

Part no	Description
1	Funnel
2	Mandrel with mold release
3	Fibre reinforcements
4	8 mm tube
5	Silicone seal
6	3 mm steel spacers

2.5. Axial compression of SMPC components

The compressive strength and failure method of the glass SMPC CHS and SHS components were evaluated in the MTS 100 kN. The length to diameter ratio (L/D) of the SMPC components was approximately 2. A displacement rate of 1.3 mm/min was used to apply a compressive load. All compressive tests were performed at room temperature.

2.6. Relaxation testing

Stress relaxation tests were carried out in a DMA Q800 for neat and reinforced SMPs. A dual cantilever fixture was used to evaluate the stress relaxing behaviour of materials within the temperature range 50 °C to 80 °C with 5 °C increment steps. Once the chamber temperature was set to a specific value, a 10 min isothermal step was used to achieve thermal equilibrium. Then, a constant strain of 0.2 % was applied and relaxation data were recorded for 15 min. The time–temperature superposition (TTS) principle was applied to characterize the viscoelastic properties of materials over an extended time period [21]. The relaxation data were analyzed with the Advantage Software (v5.5.22) rheology module, and Prony relaxation master curves were generated using Williams-Landel-Ferry (WLF) curve shifting technique [22]. The master curve was fitted with the Prony series formula described by the Generalized Maxwell Model given in Equation (1), and was used to evaluate Prony coefficients (E(t)). The shear (G(t)) and bulk moduli (K(t)) required to fully define the viscoelastic properties in ABAQUS were evaluated using Equations (2) and (3). The terms t, τ and υ represent time, relaxation time and Poisson's ratio, respectively.

$$E(t) = E_\infty + \sum_{i=1}^{n} E_i e^{-\frac{t}{\tau_i}} \tag{1}$$

$$G(t) = \frac{E(t)}{2(1+\upsilon)} \tag{2}$$

$$K(t) = \frac{E(t)}{3(1-2\upsilon)} \tag{3}$$

2.7. Shape memory effect testing

To demonstrate the shape memory behaviour of the fully cured SMPC structural components, 60 mm long components were cut and programmed by a radial distributed force along their lengths. As the deformation occurs radially, a similar shape programming behaviour can be expected even in longer specimens. Programming was carried out at a storage modulus onset (T_S = 60 °C) which was concluded from previous studies [19]. The experimental setup including the thermal chamber, fixtures and specimen positioning are illustrated in Fig. 4. Prior to the application of programming force, the SMPC structural

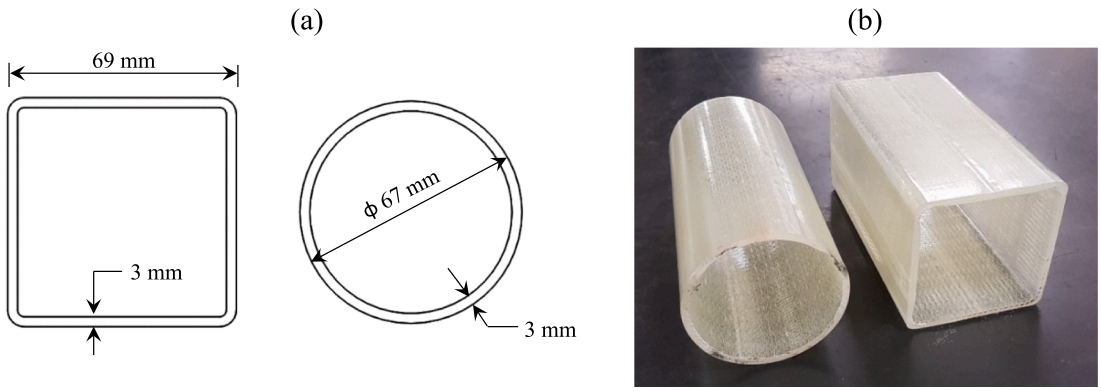

Fig. 3. Fabricated CHS and SHS components; (a) cross sectional dimensions (b) 60 mm long components tested for SME.

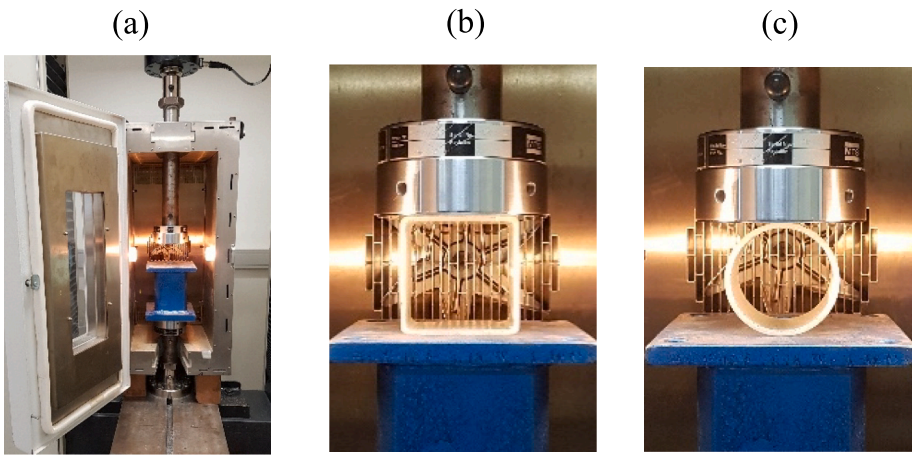

Fig. 4. SME testing of SMPC components; (a) experimental setup (b) SHS and (c) CHS components prior to programming.

components were held inside the thermal chamber of the MTS 100 kN for 30 min to achieve thermal equilibrium. Next, force was applied with a crosshead movement of 1 mm/s. During the programming stage, the time taken to initiate damage and specific locations were monitored and used to validate the FEA predictions based on the critical stress margins (CSMs) proposed in our recent studies [19]. The programming stage was terminated when the load reading on the MTS began dropping rapidly due material failure such as cracks. Then, the chamber was opened for natural cooling allowing the specimen to cool gradually from 60 °C to room temperature. Next, the applied force was removed allowing the component to spring back and fix its shape. Finally, the specimen was placed in an oven heated to 90 °C, allowing it to recover the initial shape. Photographs of the initial, fixed and recovered shapes of the components were taken to evaluate the SME properties of fixity (R_f) and recovery ratios (R_r). Moreover, Equations (4) and (5) were used to evaluate R_f and R_r [23]. The notations D1, D2, L1 and L2 denote initial height, final height, deformation and fixed deformation, respectively, and are illustrated in Fig. 5.

$$R_f = \frac{L_2}{L_1} \times 100\% \tag{4}$$

$$R_r = \frac{D_2}{D_1} \times 100\% \tag{5}$$

3. Results and discussion

3.1. Fatigue behaviour

Due to different environmental conditions, the structural components used in constructions can experience cyclic loading that can lead to a catastrophic destruction with time. Fatigue failure is induced via critical loading patterns which are lower than the ultimate strength (S_{UTS}) of materials. The fatigue behaviour of any material is very complex and challenging to predict. However, it is vital to have an understanding of how SMPCs behave under fatigue loading to analyze and investigate their applicability to proposed applications. Thus, constant amplitude axial tension–tension fatigue tests were performed for the optimized glass and basalt SMPCs for r ranging from 40 % to 80 % of S_{UTS}. These experimental results allow the identification of the fatigue strength (S_n) of the SMPC which is the safe stress margin under cyclic loading.

Fig. 6 illustrates the fatigue lifetimes of the glass and basalt SMPCs under tested load percentages. The S-N curves of these SMPCs show a similar trend compared to the fatigue behaviour of other common materials [24 25]. During fatigue testing, as per ASTM D3479/D3479M-19, the complete separation of SMPC samples was used as the criterion for

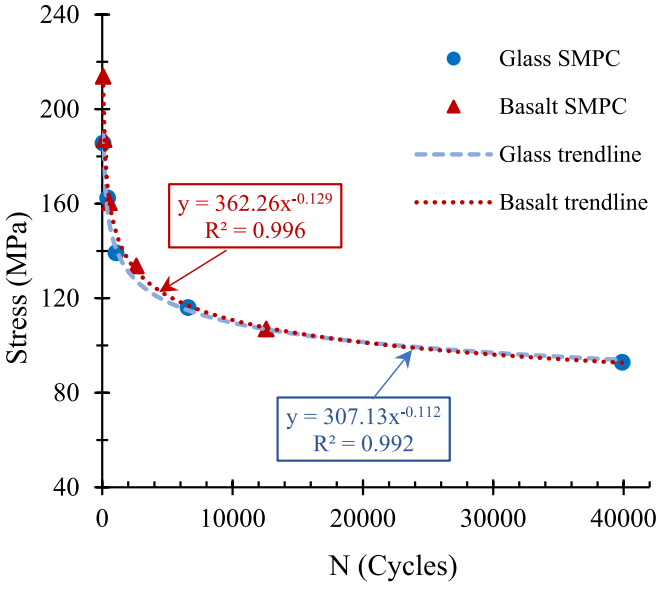

Fig. 6. S-N fatigue life characteristics for SMPCs.

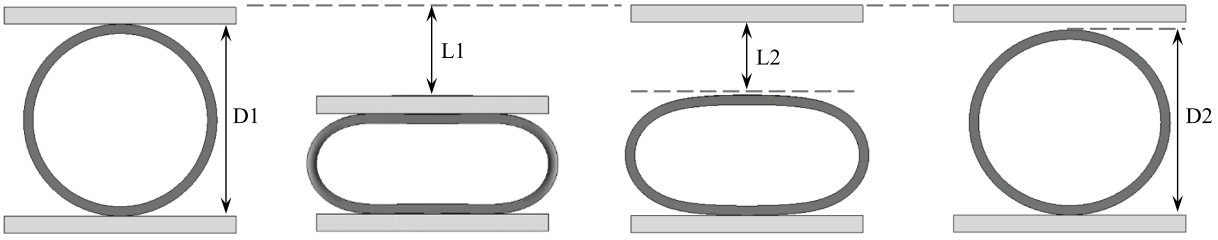

Fig. 5. Parameters used for evaluation of R_f % and R_r %.

failure. At a given load percentage, the average value of the number of cycles to failure of each sample type was used to plot the S-N curve. Subsequently, power law equations were fitted to test results and the fatigue endurance limits of the SMPCs at $2x10^6$ cycles were evaluated. The divergences between the experimental and predicted results of glass and basalt SMPCs were calculated using the correlation index (R^2), and the obtained results were 99.2 % and 99.6 %, respectively [26,27]. A fatigue life of $2x10^6$ cycles was selected as per similar fatigue studies performed for fibre reinforced plastic (FRP) [28–30] and lightweight concrete [31] for civil applications. Interestingly, basalt fibre reinforced SMPCs showed a slightly better performance under high tensile fatigue loading. In contrast, glass SMPCs exhibited marginally better resistance against lower fatigue loads. Accordingly, the endurance limit for 2 million cycles of glass and basalt SMPCs were evaluated as 60.5 MPa and 55.7 MPa, respectively (given in Table 3). Moreover, the samples have shown similar failure modes in comparison to previous studies on general polymer composites. Thus, tested SMPCs showed progressive damage failure behaviour by means of matrix cracking, fiber–matrix debonding, delamination and fiber breakage [24,25,32,33]. In addition, it was clearly seen that the fatigue failure modes of SMPCs were identical to that of the static tensile load failure mode which was also presented by Wang et al., for glass fibre reinforced epoxy composite embedded with shape memory alloy wires [33].

As mentioned previously, fatigue tests were performed at r = 0.1 with a 1 Hz frequency. However, in real life situations r and f can have different values. Using the empirical model proposed by Epaarachchi et al. [34], S-N fatigue characteristics for variable r and f values can be predicted by evaluating two material specific model parameters α and β. In addition, it is possible to avoid repeated testing for different load cases and frequencies, saving both time and effort by adhering to this method. Thus, only a few straightforward fatigue tests are required at one r value for a number of load levels to calculate α and β [34]. Therefore, following the proposed technique, respective material specific parameters were evaluated, and are illustrated in Fig. 7 and Table 4. Using the evaluated α and β values, fatigue S-N characteristic curves were generated for r values ranging from 0.1 to 0.6 (in Fig. 8). The model has shown excellent correlation with the experimental results for r = 0.1, thus showcasing its effectiveness. Importantly, based on these results, SMPC fatigue behaviour under different real life applications can be studied and predicted with ease. Hence, these results will be vital for future SMPC structural component design, ensuring they are safe and can withstand fatigue loads under operating conditions.

3.2. Axial compressive properties

Depending on their application, structural components often experience compressive loads. Thus, buckling is an important phenomenon that needs to be investigated when components are exposed to compressive stresses. Consequently, the behaviour and damage mode of the SMPC CHS and SHS components was investigated for components with L/D = 2, and are shown in Fig. 9. The CHS SMPC components showed a compressive strength of 124.7 MPa when the edges began to experience damage due to crushing. However, the SHS SMPC components experienced local buckling due to compression, and initiated damage at 69.6 MPa. This can be attributed to the stress concentration at the corners of SHS SMPC specimens, resulting a lower compressive strength compared to CHS SMPCs. Importantly, recent studies of glass fibre reinforced geopolymer concrete beams used as construction materials showed similar compressive strengths in the range 40 MPa − 85 MPa [35–37]. The comparability of the experimentally evaluated compressive strengths of the SMPC components can be further validated with respect to the results presented for FRP, concrete and steel integrated, tubular and SHS components [38,39]. Thus, the results of the compressive behaviour analysis indicate that the comparative loading capacity of the SMPC components is suitable for construction applications.

Table 3
Fatigue lives of the SMPCs.

Material	Fatigue life (million cycles)	Fatigue/Endurance limit	
		L (%)	S (MPa)
Glass SMPC	2	26	60.5
Basalt SMPC		21	55.7

3.3. Viscoelastic properties

When the SMP is heated to its T_g, the material transforms its state from solid to rubbery through a transition phase. Hence, in order to simulate the behaviour of the SMP within the phase transition region, characterization of the viscoelastic properties is essential. The generated Prony series curves for all tested specimens are presented in Fig. 10. The relaxation values taken from the Prony series of a certain material at different time values were used to define viscoelastic properties of the SMPCs in ABAQUS software. Importantly, it can be seen that both the glass and basalt fibre SMPCs showed higher relaxation moduli compared to the neat SMP. This can be attributed to the high stiffness attained with improved mechanical performance by reinforcement inclusion and low matrix content. The viscoelastic FEA modelling enables simulation of the complete thermomechanical cycle of SMPCs, and was inspired by a study conducted by Azzawi et al. [22]. In our recent studies [19], modelling of the general shape memory cycle was modified by the inclusion of tensile properties at the programming temperature to study the stress variations during programming and identify damage onset.

3.4. Modelling SME of CHS and SHS components

To improve SMPC component design and applicability in a broad spectrum of civil engineering applications, the programming stage modelling of the SMPC members is vital. FEA analysis of the SMPC component's programming stage allows the prompt prediction of any damage through stress build up, detection of critical locations prone to high stresses, determination of fibre orientation (at compressed side), evaluation of required external forces and optimization of programming process parameters, saving both time and cost. FEA and experimental shape comparisons of CHS and SHS SMPC components during programming are presented in Fig. 11 and Fig. 12, respectively. The shapes of the deformed components during the first 12 s of programming are presented. It is evident that the shapes predicted by FEA matches well with experimental deformed shapes of both tested components. In addition, the FEA model was able to demonstrate the spring back effect during shape fixing and recovery of the initial shape once thermal load is reapplied. The spring back effect can be demonstrated in the FEA model with the help of two additional visco steps for sample cooling and external force removal. Fixity and recovery ratios evaluated according to Equations (1) and (2) are given in Table 5. The evaluated ratios show a good match among FEA and experimental results, with an error percentage less than 5.6 % and 3.5 % for fixity and recovery, respectively, further validating the FEA model used. The slight difference between these results can be attributed to the material damage experienced during experimental programming.

3.4.1. Programming stage damage predictions

As per the guidelines proposed in our previous study [19], 70 MPa and 100 MPa were proposed as the critical stress limits for the SMPC during programming. In addition, Type 1 damage which corresponds to matrix-fibre debonding due to interfacial failure dominates in the stress range 70 MPa to 100 MPa. Beyond 100 MPa, the material can experience delamination and also cracks initiating on the tensioned side. Consequently, these CSMs were used to predict whether damage had occurred during the programming stage or not, and to further determine the

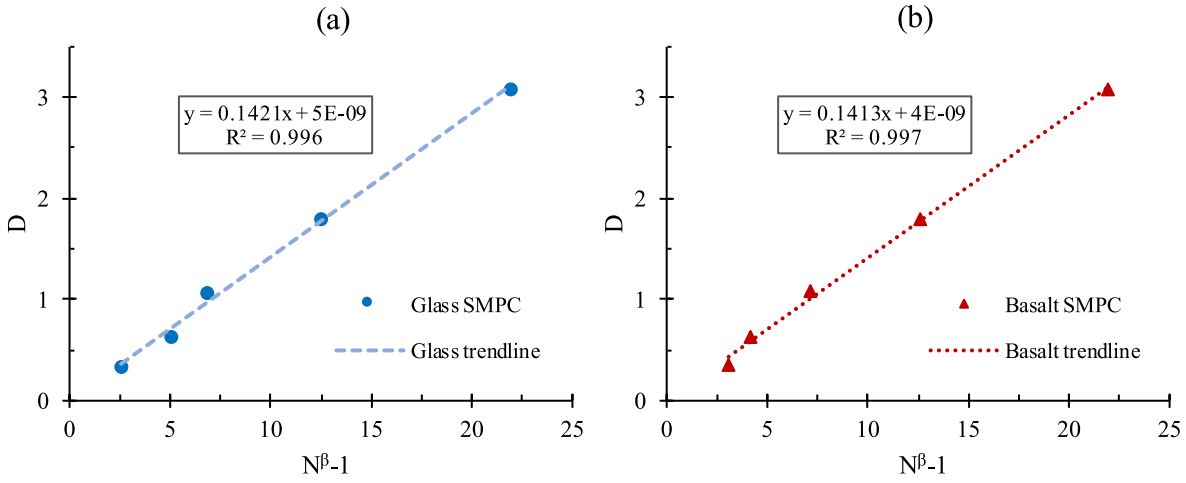

Fig. 7. Evaluation of fatigue characteristic empirical model parameters for (a) glass SMPC and (b) basalt SMPC.

Table 4
Material specific fatigue parameters.

Specimen	α	β
Glass SMPC	0.1421	0.2953
Basalt SMPC	0.1413	0.3319

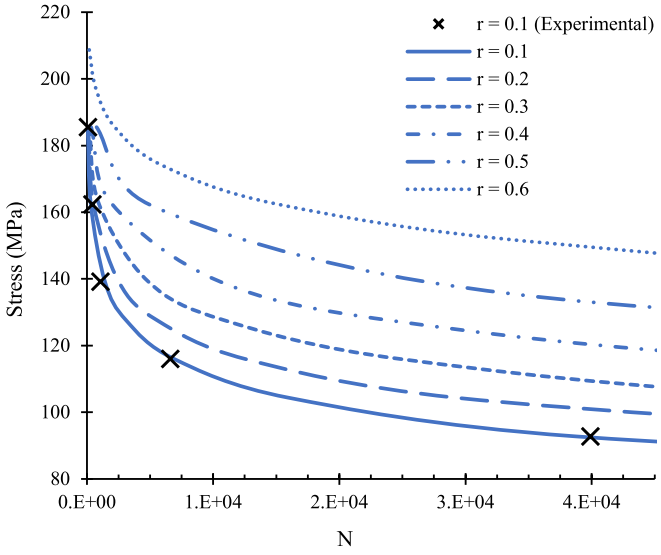

Fig. 8. Predicted S-N fatigue curves of glass SMPC for different stress ratios.

validity of the model by comparison with the experimental data. For clarity, only the damage prediction of the CHS components are presented.

Fig. 13 illustrates the variation in externally applied load (experimental) during the CHS sample programming and numerical normal stress results at the top (S11) and side (S22) of the specimen. The MTS load reading was utilized in order to recognize the initiation of material damage. As per previous studies, it was suggested that Type 2 delamination and Type 3 cracks could occur beyond a 100 MPa stress level. The material damage Types 2 and 3 refer to delamination and through thickness cracking, respectively. The sudden drop in the experimental load curve in Fig. 13 is a result of the initiation of a crack or considerable material damage. The CHS specimen has experienced material damage during the process of programming when it was deformed by 31.2 mm. The FEA stress level on the side of the CHS sample reached 100 MPa close to 32 mm. As per developed stresses (Fig. 13) on top and side of the CHS, the top should experience Type 1 and the side should undergo damage Types 2 and 3. Interestingly, these simulation based results showed good consistency with experimentally experienced damage types and are shown in Fig. 14. This proves the effectiveness of the proposed CSMs to numerically investigate and predict the likelihood of material damage during programming. Moreover, most critical locations of the SMPC component prone to damage can also be detected with ease.

In the SHS SMPC samples, a rapid drop in applied test load was seen at a displacement of 11.3 mm, whereas from the FEA results, normal stress on the damaged side achieved 100 MPa at 10.6 mm, demonstrating good consistency with the proposed framework (damage onset at 70 MPa). According to the radial deformability results of the SMPC sections, the SHS showed a quick damage onset at a lower deformation. Hence, the SHS sections can be categorized as more critical compared to CHS which can result in programming damage easily. Consequently, in this paper, SMPC application suggestions are presented considering only SHS SMPC members.

3.5. *Application of SMPCs in long beams and deployable structures*

a) SMPC long beams.

SMPC SHS and CHS structural components can be used in many challenging civil engineering applications because of their unique intrinsic properties. They can be deformed easily at low cost and with minimal labour to a temporary or confined shape, and then transported to the construction site with ease. Finally, by applying the external stimulus, the deformed SMPC components and structures can be recovered to their initial shapes wherever required. Some suitable engineering applications for these smart SHS and CHS structural components are prefabricated modular constructions, construction of footbridges in remote areas, constructions in challenging terrain, as an alternative to expensive and heavy curved steel beams, for deployable lunar habitats and outer space structures.

The shape memory performance of a large scale 5 m long SHS SMPC member, with the cross section given in Fig. 3 (a), was also investigated via FEA. A displacement boundary condition was applied at the mid span of the SMPC member at 1 mm/s deformation rate. The deformation rate was identified from our recent studies [19]. To demonstrate the shape deformability of the SMPC members, only the FEA analysis for the SHS SMPC is presented here for clarity. The SHS components initiated damage at a lower radial displacement as described in Section 3.4.1. The FEA analysis was performed for different support spans (S) and mid span displacements (D). Subsequently, the developed maximum compressive bending stress and bend radius (R) of the SMPC member was evaluated

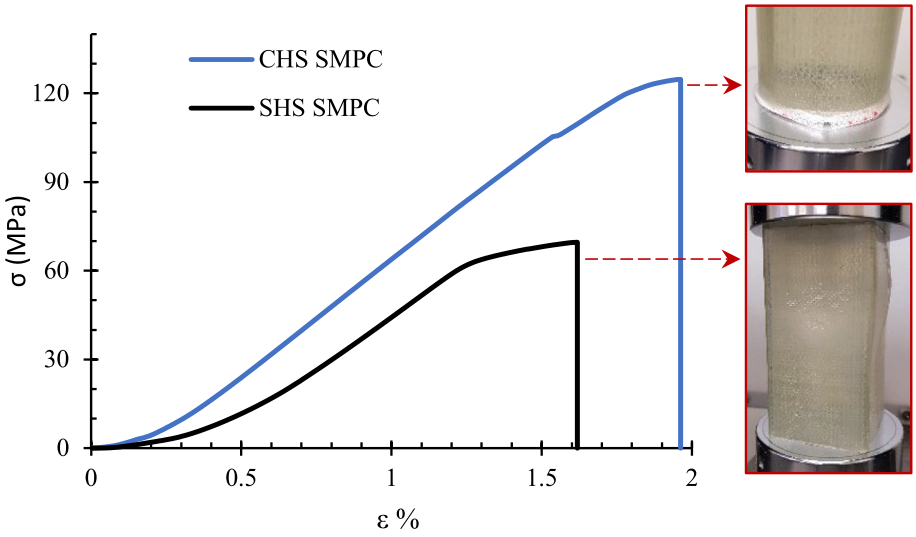

Fig. 9. Behaviour of CHS and SHS glass SMPCs under axial compression.

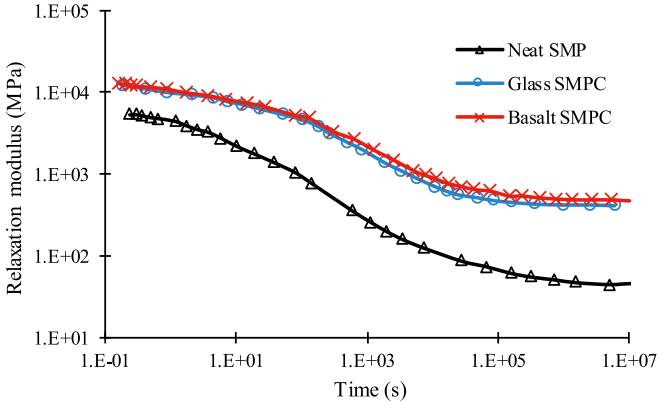

Fig. 10. Relaxation Prony series curves for neat SMP and SMPCs.

for analysis. As the compressive side of the SMPC is prone to damage during the programming stage, the compressive stress was used as the tool to predict damage onset.

FEA viscoelastic simulations were performed for five S values and deformed to a maximum of D = 1000 mm. The summary of FEA results is presented in Fig. 15. Interestingly, for S > 1000 mm, the compressive stress was below 70 MPa for all D values. However, the evaluated stress exceeded damage onset stress (σ_o) when S = 1000 mm. Hence, the span of 1000 mm can be identified as the critical span (S_C) value for SHS programming. Moreover, for the configuration with S_C, the R values of the deformed SMPC members were evaluated (in Fig. 16) to determine the limiting bend radius. According to the recognized relationship between R and compressive stress, 650 mm was revealed as the critical bend radius (R_C) for SHS SMPC member programming. Hence, it demonstrates the ability of the fabricated SMPC SHS components to be deformed or wrapped to a compact temporary shape with a bend radius of 650 mm (1.3 m diameter). Similarly, from the FEA study performed for a 5 m long CHS SMPC beam, the R_C was evaluated as 420 mm (0.84 m diameter) for the same S_C. Further, it is clear that CHS SMPC members showed better shape memory performance in comparison to SHS sections, with respect to undamaged shape deformability. These tightly wrapped long SMPC CHS and SHS members can even be stored in a car for transportation as the average width of a passenger car is around 1.75 m [40].

b) Deployable SMPC structures.

To demonstrate the application of large scale SMPC structural

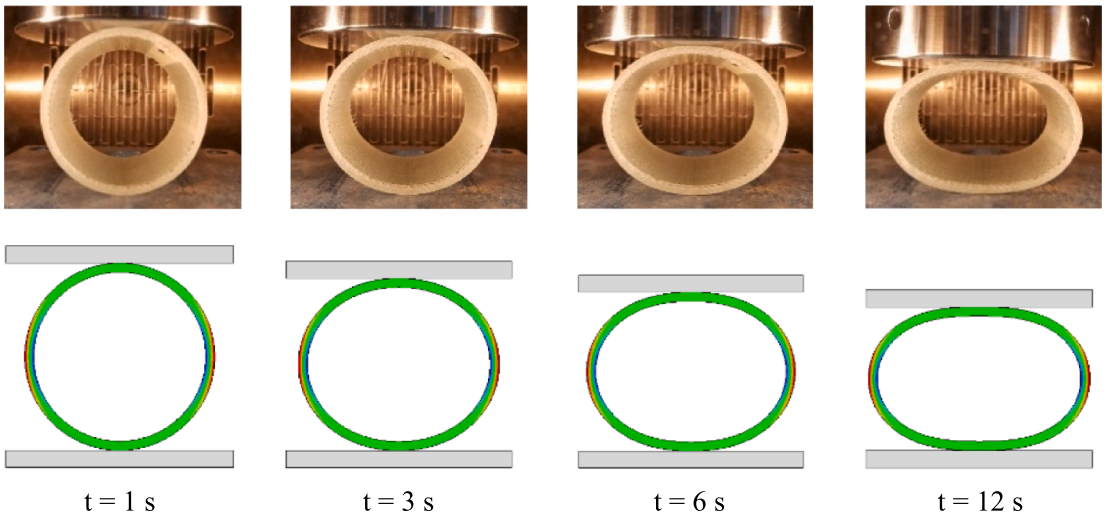

Fig. 11. Shape comparison of CHS SMPC components during first 12 s of programming.

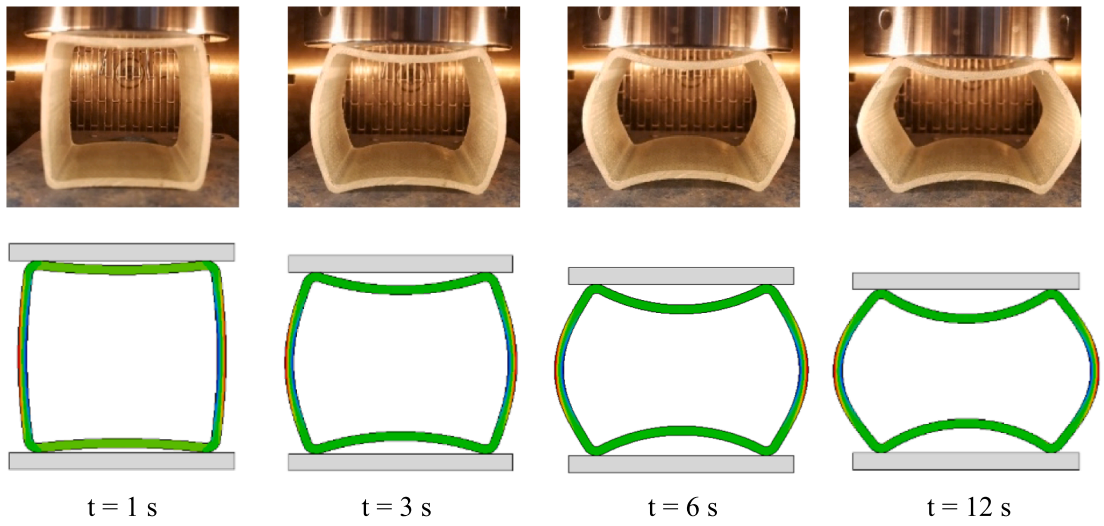

Fig. 12. Shape comparison of SHS SMPC components during first 12 s of programming.

Table 5
Experimental and FEA fixity and recovery values.

Component	Programming displacement (mm)	Method	R_f %	R_r %
SHS	15	Experimental	72.6	96.5
		FEA	68.5	99.9
CHS	32	Experimental	82.1	98.1
		FEA	78.8	99.8

components in deployable structures, a 5x5x5 m^3 frame structure was analyzed numerically with CHS and SHS members, separately. Fig. 17 illustrates the shape programming of a single SHS and CHS vertical strut of the structure, up to a maximum compressive stress (S33) of approximately 70 MPa to ensure no damage occurred. The initial lengths of both members were 5 m. According to the results, the SHS and CHS SMPC members experienced overall length reductions of 2.6 m and 3.5 m, respectively, with no programming damage. Thus, the height of the SMPC structure has reduced to 2.4 m and 1.5 m, respectively for SHS and CHS. The overall compact configuration of the SHS structure with four programmed struts is presented in Fig. 18. A volume reduction of 52 % and 70 % was achieved by the SHS and CHS structures, respectively. Table 6 presents the initial (Vi) and final (Vf) volumes of the two SMPC structures. Importantly, the results clearly show the space saving advantage that can be achieved by SMPC integration into structural components. In contrast to traditional construction materials and technologies, the use of SMPC structural members can be a game changer for prefabricated modular constructions, heavy curved steel structures, space deployable structures, lunar habitats, foot bridges, etc.

c) Nominal section capacities of SMPC members.

According to the steel designer's handbook [41] and Australian standard AS 4100 [42], the suitability of structural members of a particular material can be assessed by calculating the nominal section capacities. The sectional capacities are categorized according to the subjected loading such as bending (AS 4100–5.2) and axial compression (AS 4100–6.2). To further demonstrate the applicability of SMPCs, the CHS structural capacity to weight ratio (specific strength) was evaluated and compared with steel. Equations (6) and (7) illustrate the nominal section capacity equation for bending and axial compression, respectively. M_S = Nominal section capacity for bending (AS4100-5.2.1), f_y = Yield strength used in design, Z_e = Effective section modulus, N_S = Nominal section capacity for axial compression (AS4100-6.2.1), k_f = Form factor, A_n = Net cross sectional area, d_o = Outer diameter, t = Thickness, ρ = Density). For both loading criteria, the CHS SMPC components demonstrated higher "specific sectional capacities"

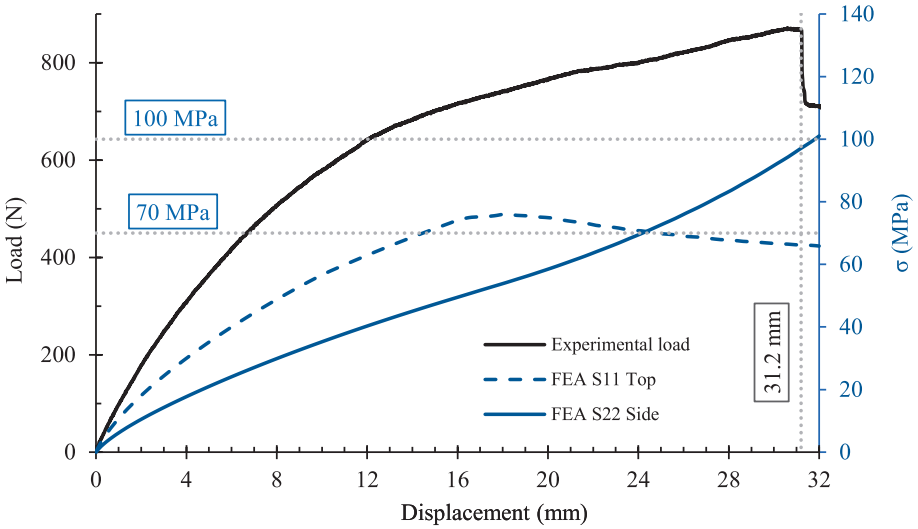

Fig. 13. Comparison of external load applied during experimental programming test and FEA compressive stress results on side and top faces of CHS components.

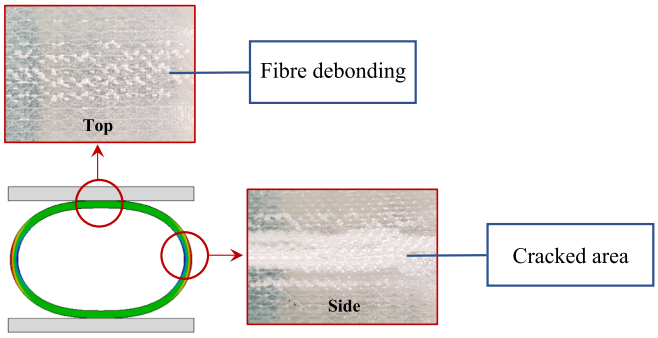

Fig. 14. Damage types on radially deformed CHS components.

showcasing their structural potential as lightweight components in comparison to heavy steel sections. The calculation results for the CHS sections are presented in Table 7.

$$\text{For bending}: M_S = f_y Z_e \tag{6}$$

$$\text{For axial compression}: N_S = k_f A_n f_y \tag{7}$$

4. Conclusion

In this paper, we demonstrated the applicability of SMPCs in real scale CHS and SHS structural components. The integration of SMPCs in commonly used members can transform their current capacity, allowing them to be deformed to a compact shape for easy transportation and handling, or incorporate curvy shapes into constructions. Importantly, FEA based damage predictions of the SMPC components were consistent with the experimental results. In addition, it was found that long SHS and CHS SMPC structural members can be wrapped to a minimum radii of 650 mm and 420 mm, respectively, without undergoing any damage during programming. Further, the application of shape deformable SMPC members was presented in a deployable structure which showcased exciting volume savings of 52 % and 70 % for SHS and CHS SMPCs, respectively. According to the tension–tension fatigue characterization, the endurance limits of the glass and basalt SMPCs at 2 million lifetime were 60.5 MPa and 55.7 MPa, respectively. Moreover, the fatigue material specific parameters (α and β) were evaluated, and S-N predictions for non-tested r values are presented. Importantly, the fatigue study contributes significant research knowledge to fill out knowledge gaps related to SMPC performance. Overall, the study provides a firsthand approach and framework to incorporate the shape memory effect of SMPCs in construction components. This novel application can aid future researchers seeking to revolutionize construction techniques, making them smarter, cheaper and quicker. As future works, it recommended to characterize SMPC properties under complex force situations and durability conditions, as a construction material.

CRediT authorship contribution statement

K.D.C. Emmanuel: Conceptualization, Methodology, Investigation, Writing – original draft. **L.H.J. Jeewantha:** Investigation, Resources. **H. M.C.M. Herath:** Writing – review & editing. **J.A. Epaarachchi:** Conceptualization, Supervision, Writing – review & editing. **T. Aravinthan:** Supervision.

Declaration of Competing Interest

The authors declare that they have no known competing financial interests or personal relationships that could have appeared to influence the work reported in this paper.

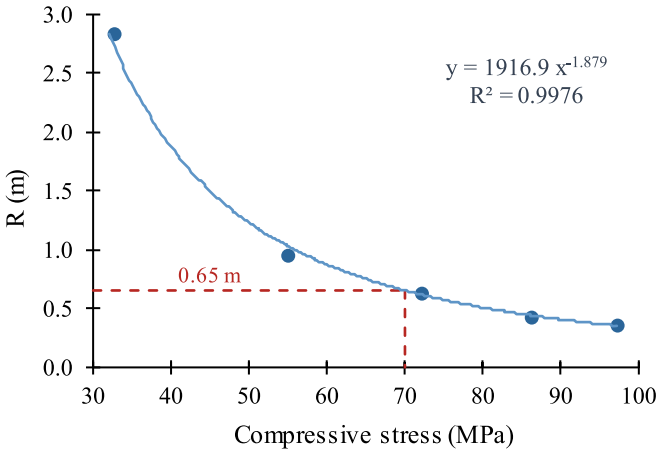

Fig. 16. Relationship between R and compressive stress for configuration with S_C.

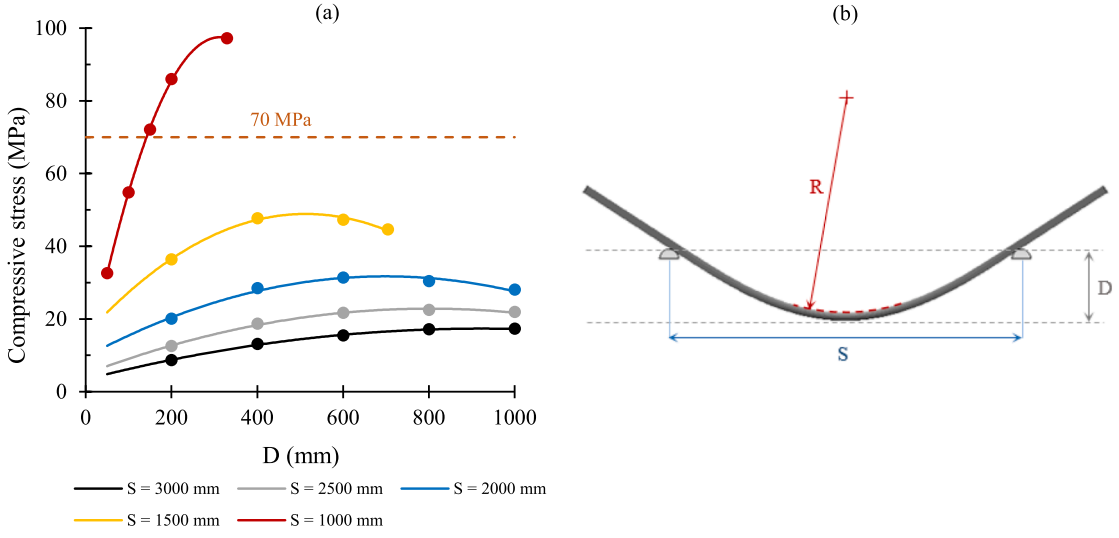

Fig. 15. FEA results summary (a) variation of compressive stress with D and S values (b) test parameters.

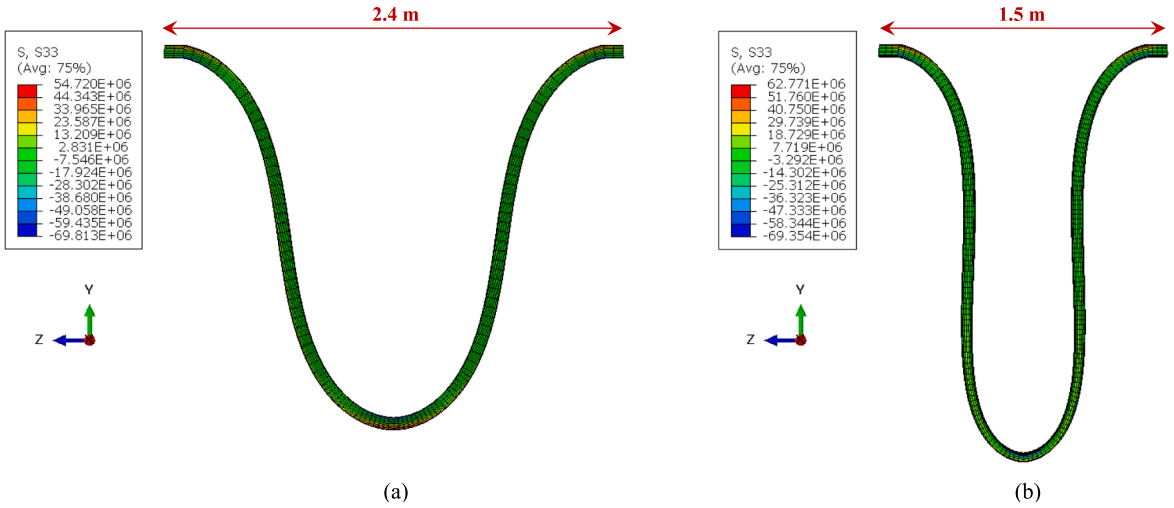

Fig. 17. Shape programming of vertical member in frame structure; (a) SHS and (b) CHS.

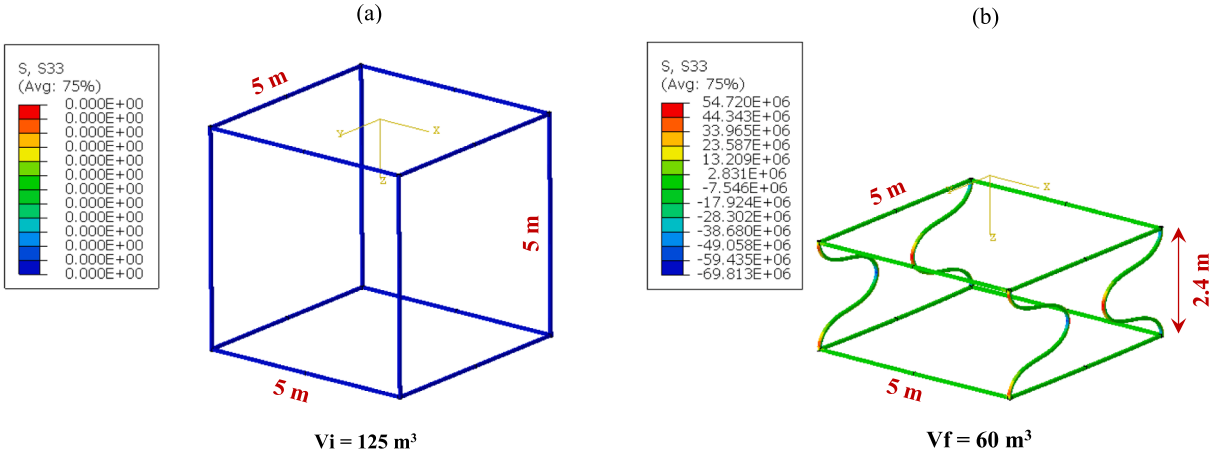

Fig. 18. SHS SMPC structure configurations; (a) initial (b) programmed.

Table 6
Volume savings of (a) SHS and (b) CHS SMPC structures.

SMPC member	Vi (m^3)	Vf (m^3)	Volume saving (%)
SHS	125	60	52
CHS	125	37	70

Table 7
CHS specific section capacity for mild steel and SMPC.

CHS	d_o (mm)	t (mm)	ρ (kg/m^3)	f_y (MPa)	M_S (Nm)	M_S/ρ	N_S/ρ
Mild steel	60.3	2.9	7800	380 [43]	4082	**0.5**	**25.5**
SMPC	67	3	1320	232	3215	**2.4**	**57.0**

Data availability

Data will be made available on request.

References

[1] Zhang H. Building materials in civil engineering. Elsevier; 2011.
[2] Duggal SK. Building materials. Routledge; 2017.
[3] A. S. Mosallam, A. Bayraktar, M. Elmikawi, S. Pul, and S. Adanur, "Polymer composites in construction: an overview," 2021.
[4] Liu Y, Du H, Liu L, Leng J. Shape memory polymers and their composites in aerospace applications: a review. Smart Mater Struct 2014;23(2):pp. https://doi.org/10.1088/0964-1726/23/2/023001.
[5] Herath HMCM, Epaarachchi JA, Islam MM, Al-Azzawi W, Leng J, Zhang F. Structural performance and photothermal recovery of carbon fibre reinforced shape memory polymer. Compos Sci Technol 2018;167:206–14. https://doi.org/10.1016/j.compscitech.2018.07.042.
[6] Jeewantha J, et al. Shape memory polymer smart plaster for orthopaedic treatments. Smart Mater Struct 2022;31(11):115016.
[7] Lendlein A, Kelch S. Shape-Memory Polymers. Angew Chem Int Ed 2002;41(12): 2034–57. https://doi.org/10.1002/1521-3773(20020617)41:12<2034::Aid-anie2034>3.0.Co;2-m.
[8] J. Jeewantha, C. Emmanuel, M. Herath, M. Islam, and J. Epaarachchi, "Development and characterization of shape memory polymers for non-invasive biomedical applications," in *Smart Materials, Adaptive Structures and Intelligent Systems*, 2021, vol. 85499: American Society of Mechanical Engineers, p. V001T02A001.
[9] Meng Q, Hu J. A review of shape memory polymer composites and blends. Compos A Appl Sci Manuf 2009;40(11):1661–72. https://doi.org/10.1016/j.compositesa.2009.08.011.
[10] Li F, Liu Y, Leng J. Progress of shape memory polymers and their composites in aerospace applications. Smart Mater Struct 2019;28(10):pp. https://doi.org/10.1088/1361-665X/ab3d5f.
[11] L. Santo, F. Quadrini, D. Bellisario, and L. Iorio, "Applications of Shape-Memory Polymers, and Their Blends and Composites," in *Shape Memory Polymers, Blends and Composites*, (Advanced Structured Materials, 2020, ch. Chapter 13, pp. 311-329.
[12] Emmanuel KDC, Herath HMCM, Jeewantha LHJ, Epaarachchi JA, Aravinthan T. Thermomechanical and fire performance of DGEBA based shape memory polymer composites for constructions. Constr Build Mater 2021;303. https://doi.org/10.1016/j.conbuildmat.2021.124442.
[13] M. Herath, C. Emmanuel, J. Jeewantha, and J. Epaarachchi, "In-situ performance evaluation of large shape memory polymer components via distributed optical

fibre sensors," in *2021 10th International Conference on Information and Automation for Sustainability (ICIAfS)*, 2021: IEEE, pp. 458-463.
[14] Leng J, Lan X, Liu Y, Du S. Shape-memory polymers and their composites: Stimulus methods and applications. Prog Mater Sci 2011;56(7):1077–135. https://doi.org/10.1016/j.pmatsci.2011.03.001.
[15] Herath HMCM, Epaarachchi JA, Islam MM, Leng J. Carbon Fibre Reinforced Shape Memory Polymer Composites for Deployable Space Habitats. Engineer: Journal of the Institution of Engineers, Sri Lanka 2019;52(1). https://doi.org/10.4038/engineer.v52i1.7323.
[16] Ferdous W, Bai Y, Ngo TD, Manalo A, Mendis P. New advancements, challenges and opportunities of multi-storey modular buildings – A state-of-the-art review. Eng Struct 2019;183:883–93. https://doi.org/10.1016/j.engstruct.2019.01.061.
[17] Thai H-T, Ngo T, Uy B. A review on modular construction for high-rise buildings. Structures 2020;28:1265–90. https://doi.org/10.1016/j.istruc.2020.09.070.
[18] Hall DH, Grubb MA, Yoo CH. Improved design specifications for horizontally curved steel girder highway bridges, no. 424. Transportation Research Board; 1999.
[19] Emmanuel KDC, Jeewantha LHJ, Herath HMCM, Epaarachchi JA, Aravinthan T. Damage onset analysis of optimized shape memory polymer composites during programming into curved shapes. Materialia 2022;26. https://doi.org/10.1016/j.mtla.2022.101599.
[20] *Standard Test Method for Tension-Tension Fatigue of Polymer Matrix Composite Materials*, A. International, 2019.
[21] W. Al Azzawi, M. Herath, and J. Epaarachchi, "Modeling, analysis, and testing of viscoelastic properties of shape memory polymer composites and a brief review of their space engineering applications," *Creep and Fatigue in Polymer Matrix Composites*, pp. 465-495, 2019.
[22] Azzawi WA, Epaarachchi JA, Islam M, Leng J. Implementation of a finite element analysis procedure for structural analysis of shape memory behaviour of fibre reinforced shape memory polymer composites. Smart Mater Struct 2017;26(12): pp. https://doi.org/10.1088/1361-665X/aa928e.
[23] Xie T. Tunable polymer multi-shape memory effect. Nature 2010;464(7286):267–70.
[24] Vieira PR, Carvalho EML, Vieira JD, Toledo Filho RD. Experimental fatigue behavior of pultruded glass fibre reinforced polymer composite materials. Compos B Eng 2018;146:69–75. https://doi.org/10.1016/j.compositesb.2018.03.040.
[25] Kukureka SN, Wei CY. Damage development in pultruded composites for optical telecommunications cables under tensile and flexural fatigue. Compos Sci Technol 2003;63(12):1795–804. https://doi.org/10.1016/s0266-3538(03)00132-5.
[26] Liu J, Xing Z, Lu H, Fu Y-Q. Interfacial confinement in semi-crystalline shape memory polymer towards sequentially dynamic relaxations. Int J Appl Mech 2021;13(10):2150117.
[27] Liu J, Gorbacheva G, Lu H, Wang J, Fu Y-Q. A dynamic hysteresis model for customized glass transition in amorphous polymer towards multiple shape memory effects. Smart Mater Struct 2022;31(12):125022.
[28] Van Den Einde L, Zhao L, Seible F. Use of FRP composites in civil structural applications. Constr Build Mater 2003;17(6–7):389–403. https://doi.org/10.1016/s0950-0618(03)00040-0.
[29] Kumar P, Chandrashekhara K, Nanni A. Structural performance of a FRP bridge deck. Constr Build Mater 2004;18(1):35–47. https://doi.org/10.1016/s0950-0618(03)00036-9.
[30] Wu Z, Wang X, Iwashita K, Sasaki T, Hamaguchi Y. Tensile fatigue behaviour of FRP and hybrid FRP sheets. Compos B Eng 2010;41(5):396–402. https://doi.org/10.1016/j.compositesb.2010.02.001.
[31] Saito M. Tensile fatigue strength of lightweight concrete. Int J Cem Compos Light Concr 1984;6(3):143–9.
[32] Colombo C, Vergani L. Multi-axial fatigue life estimation of unidirectional GFRP composite. Int J Fatigue 2011;33(8):1032–9. https://doi.org/10.1016/j.ijfatigue.2011.01.001.
[33] Wang Z, Xu L, Sun X, Shi M, Liu J. Fatigue behavior of glass-fiber-reinforced epoxy composites embedded with shape memory alloy wires. Compos Struct 2017;178:311–9. https://doi.org/10.1016/j.compstruct.2017.07.027.
[34] Epaarachchi JA, Clausen PD. An empirical model for fatigue behavior prediction of glass fibre-reinforced plastic composites for various stress ratios and test frequencies. Compos A Appl Sci Manuf 2003;34(4):313–26. https://doi.org/10.1016/s1359-835x(03)00052-6.
[35] Srinivasa Rao P, SeshadriSekhar T, Sravana P. Strength properties of glass fibre concrete. ARPN Journal of Engineering and Applied Sciences 2010;5(4):1–6.
[36] Shakor PN, Pimplikar S. Glass fibre reinforced concrete use in construction. Int J Technol Eng Syst 2011;2(2):pp.
[37] Maranan GB, Manalo AC, Benmokrane B, Karunasena W, Mendis P. Evaluation of the flexural strength and serviceability of geopolymer concrete beams reinforced with glass-fibre-reinforced polymer (GFRP) bars. Eng Struct 2015;101:529–41. https://doi.org/10.1016/j.engstruct.2015.08.003.
[38] Teng JG, Yu T, Wong YL, Dong SL. Hybrid FRP–concrete–steel tubular columns: Concept and behavior. Constr Build Mater 2007;21(4):846–54. https://doi.org/10.1016/j.conbuildmat.2006.06.017.
[39] Bambach MR, Jama HH, Elchalakani M. Axial capacity and design of thin-walled steel SHS strengthened with CFRP. Thin-Walled Struct 2009;47(10):1112–21. https://doi.org/10.1016/j.tws.2008.10.006.
[40] Furth PG, Dulaski DM, Buessing M, Tavakolian P. Parking lane width and bicycle operating space. Transp Res Rec 2010;2190(1):45–50.
[41] Gorenc B, Gorenc BE, Tinyou R, Syam A. Steel designers' handbook. UNSW Press; 2005.
[42] *AS 4100 - Steel Structures*, S. Australia, 2020.
[43] Alhassan E, Olasehinde D, Musonda A, Odeniyi O. Tensile and flexural behaviour of steel materials used in the construction of crop processing machines. In: IOP Conference Series: Earth and Environmental Science, vol. 445, no. 1. IOP Publishing; 2020. p. 012044.